BIOCHEMISTRY
including biophysical chemistry & molecular biology

Article

pubs.acs.org/biochemistry

High-Frequency Electron Nuclear Double-Resonance Spectroscopy Studies of the Mechanism of Proton-Coupled Electron Transfer at the Tyrosine-D Residue of Photosystem II

Ruchira Chatterjee,[†] Christopher S. Coates,[†] Sergey Milikisiyants,[†] Cheng-I Lee,[§] Arlene Wagner,[‡] Oleg G. Poluektov,[‡] and K. V. Lakshmi*[,†]

[†]Department of Chemistry and Chemical Biology and The Baruch '60 Center for Biochemical Solar Energy Research, Rensselaer Polytechnic Institute, Troy, New York 12180, United States

[‡]Chemical Sciences and Engineering Division, Argonne National Laboratory, 9700 South Cass Avenue, Argonne, Illinois 60439, United States

[§]Department of Life Science, National Chung Cheng University, 168 University Road, Min-Hsiung, Chia-Yi 621, Taiwan

ABSTRACT: The solar water-splitting protein complex, photosystem II, catalyzes one of the most energetically demanding reactions in Nature by using light energy to drive the catalytic oxidation of water. Photosystem II contains two symmetrically placed tyrosine residues, Y_D and Y_Z, one on each subunit of the heterodimeric core. The Y_Z residue is kinetically competent and is proposed to be directly involved in the proton-coupled electron transfer reactions of water oxidation. In contrast, the Y_D proton-coupled electron transfer redox poises the catalytic tetranuclear manganese cluster and may electrostatically tune the adjacent monomeric redox-active chlorophyll and β-carotene in the secondary electron transfer pathway of photosystem II. In this study, we apply pulsed high-frequency electron paramagnetic resonance (EPR) and electron nuclear double-resonance (ENDOR) spectroscopy to study the photochemical proton-coupled electron transfer (PCET) intermediates of Y_D. We detect the "unrelaxed" and "relaxed" photoinduced PCET intermediates of Y_D using high-frequency EPR spectroscopy and observe an increase of the *g* anisotropy upon temperature-induced relaxation of the unrelaxed intermediate to the relaxed state as previously observed by Faller et al. [(2002) *Biochemistry 41*, 12914−12920; (2003) *Proc. Natl. Acad. Sci. U.S.A. 100*, 8732−8735]. This observation suggests the presence of structural differences between the two intermediates. We probe the possible structural differences by performing high-frequency ^{2}H ENDOR spectroscopy experiments. On the basis of numerical simulations of the experimental ^{2}H ENDOR spectra, we confirm that (i) there is a significant change in the H-bond length of the tyrosyl radical in the unrelaxed (1.49 Å) and relaxed (1.75 Å) PCET intermediates. This observation suggests that the D2-His189 residue is deprotonated prior to electron transfer at the Y_D residue and (ii) there are negligible changes in the conformation of the tyrosyl ring in the unrelaxed and relaxed PCET intermediates of Y_D.

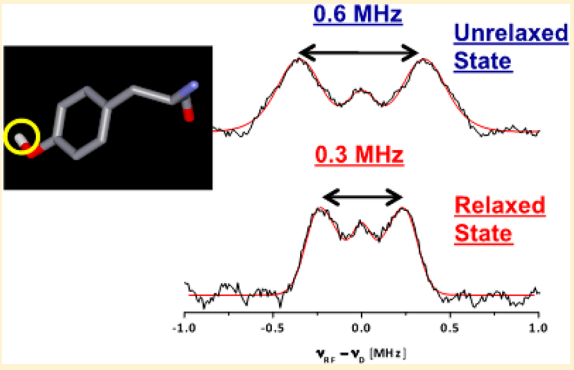

The versatility of charge transfer processes in biological energy transduction is demonstrated by the photosynthetic reaction centers (RCs) that are present in plants and bacteria.[1] In particular, light-induced proton-coupled electron transfer (PCET) reactions are of central importance in the energetics of photosynthetic type II RCs.[2] PCET reactions are also known to participate in small-molecule activation, redox-driven proton pumps, and hydrogen atom abstraction in a variety of proteins.[3]

PCET reactions are vital for the solar water oxidation reaction of photosystem II (PSII).[1] PSII catalyzes one of the most energetically demanding reactions in Nature by using light energy to drive a catalyst capable of oxidizing water.[4−9] In PSII, PCET reactions diminish the large energetic penalty for the multielectron (4e) transfers that are required for the oxidation of water to dioxygen by the coupling of proton (PT) and electron transfer (ET) processes. Thus, PCET greatly enhances the electrochemical driving force of the water oxidation reaction of PSII.[10,11] This is important as PCET reactions hold a great deal of potential for the design of bioinspired systems for solar fuel production. The major challenges at present are in attaining the high efficiency of the early charge transfer steps and understanding the role of PCET reactions in natural photosynthesis. However, the mechanistic details of PCET are lacking because of the inability of current methods to directly probe these reactions in natural photosynthetic systems.

Received: September 5, 2012
Revised: June 12, 2013
Published: June 17, 2013

The solar water oxidation reaction of PSII results from PCET reactions at the redox-active tyrosine and quinone cofactors.[12] These cofactors have the remarkable ability to control and modulate ET and PT chemistry in PSII. It is thought that the location of the cofactor, the geometry of its binding site, the redox potential, and dynamics from the surrounding protein environment greatly influence the unrivaled efficiency of PCET reactions in the photochemical reactions of PSII. To understand the mechanisms and the versatility of PCET reactions, we need to understand the factors that control the functional tuning of these cofactors. The recent 1.9−3.8 Å resolution X-ray crystal structures reveal atomic-level information about the dark state of PSII.[13−19] The preliminary information available from the X-ray crystal structures sets the stage for the development and application of state-of-the-art magnetic resonance spectroscopy methods for interrogating the molecular basis of the light-driven PCET reactions of PSII.

PSII contains two symmetrically placed tyrosine residues, Y_D and Y_Z, on each subunit of the heterodimeric polypeptide core.[12,20] The function of the symmetry-related tyrosine residues is quite distinct as the protein environment greatly influences tyrosine function in PSII. It is proposed that the PCET redox at Y_D poises the catalytic Mn_4Ca cluster[21] and may electrostatically tune the adjacent monomeric redox-active chlorophyll and β-carotene in the secondary ET pathway of PSII.[22,23] In contrast, Y_Z is kinetically competent and directly involved in the PCET reactions of the water oxidation reaction of PSII.[24,25] The redox-active tyrosine residues of PSII are especially attractive as an experimental system because (a) Y_Z and Y_D have distinct properties, including time scales and specificity of redox activity, and (b) the PCET reactions at Y_Z and Y_D can be studied at cryogenic temperatures.[26,27]

Electron paramagnetic resonance (EPR) and electron nuclear double-resonance (ENDOR) spectroscopy are powerful tools for the study of the structure and dynamics of paramagnetic centers in photosynthetic RCs.[28−30] In ENDOR spectroscopy, the nuclear resonance frequencies are monitored indirectly through EPR transitions. Typically, the nuclear transitions detected in an ENDOR spectroscopy experiment have sensitivities higher than those of conventional nuclear magnetic resonance (NMR) detection and higher selectivity because of detection through the electron spin. In addition, the application of high-frequency (HF) EPR spectroscopy methods provides enhanced sensitivity and **g** tensor resolution. The application of ENDOR spectroscopy at high frequency facilitates the detection of weak electron−nuclear interactions and affords orientation selection that can remove interactions from overlapping signals. This provides accurate information about the interaction of the radical with the surrounding protein environment.[31]

Previous studies have used EPR spectroscopy to illustrate the presence of photoinduced intermediates of the Y_D residue of PSII.[26,27,32−35] It was demonstrated that photo-oxidation of Y_D at 7 K results in the formation of the low-temperature early "unrelaxed" PCET intermediate of $Y_D^\bullet$ where the proton and protein motion are limited. The illumination of PSII at a higher temperature (240 K) allows for unrestricted proton movement and possibly the relaxation of the protein environment that leads to the formation of the late "relaxed" PCET intermediate of $Y_D^\bullet$.[26,27] These studies identified changes in the **g** tensor of the unrelaxed and relaxed intermediates that were suggested to arise from a change in the hydrogen bond distance of the $Y_D^\bullet$ radical. However, it was not possible to disentangle the hydrogen bond changes and possible conformational effects of Y_D in the unrelaxed and relaxed intermediate of the $Y_D^\bullet$ radical.

In this study, we demonstrate the application of pulsed HF EPR and HF ^{2}H ENDOR spectroscopy to obtain structural details of the unrelaxed and relaxed photoinduced PCET intermediates of the Y_D residue of PSII. A combination of electron transfer, proton movement, and local conformational effects of $Y_D^\bullet$ can result in PCET reactions in the oxygen-evolving complex (OEC) of PSII. We report pulsed HF ^{2}H ENDOR measurements of the hydrogen (H)-bonded deuteron of $Y_D^\bullet$, which provides quantitative knowledge of the H-bond strength and proton movement in the respective PCET intermediates.[36] We also report HF ^{2}H ENDOR measurements of deuterons at the 2, 6 ring and β-methylene positions of $Y_D^\bullet$ that yield information about the relative geometry of the tyrosine ring in the PCET intermediates.

In this study, we observe changes in the H-bond strength from possible conformational effects during photoinduced PCET at the tyrosine-D residue of PSII that cannot be discerned by other structural methods. The results provide important insight into the mechanism of PCET at the tyrosine-D residue of photosystem II.

MATERIALS AND METHODS

Preparation of Photosystem II. *Preparation of Deuterated Photosystem II from Synechococcus lividus.* The *S. lividus* cells were grown at 43 °C in deuterated Ac medium.[37] The photosystem II (PSII) core complexes were isolated from the deuterated cells using the procedure of Tang and Diner[38] with minor modifications.[37] The cell extract containing deuterated PSII was loaded onto a diethylaminoethyl (DEAE) cellulose ion-exchange column (Tosoh Biosciences, King of Prussia, PA) in the absence of magnesium sulfate ($MgSO_4$), and the PSII was eluted with a 1 L gradient from 0 to 50 mM $MgSO_4$ in buffer containing 50 mM 2-(*N*-morpholino)-ethanesulfonic acid (MES-NaOH), 20 mM calcium chloride ($CaCl_2$), and 5 mM magnesium chloride ($MgCl_2$) at pH 6.0 with 25% (w/v) glycerol and 0.03% (w/v) dodecyl β-D-maltoside (β-DM).[37] The deuterated PSII fractions were collected and concentrated to a volume of 2 mL. The concentrated eluent was desalted using an EconoPac 10 D6 desalting column (Bio-Rad, Hercules, CA). Following this, the deuterated PSII was resuspended in buffer containing 50 mM MES-NaOH, 20 mM $CaCl_2$, and 5 mM $MgCl_2$ at pH 6.0 with 25% (w/v) glycerol and 0.03% (w/v) β-DM. The purified deuterated PSII was characterized using 12% sodium dodecyl sulfate−polyacrylamide gel electrophoresis (SDS−PAGE) analysis. The isolation and purification of deuterated PSII were performed in the dark at 4 °C, and the samples were stored at −80 °C in the dark until further use.

Preparation of Histidine-Tagged (HT) Photosystem II from the PsbB Variant of Synechocystis PCC 6803. The PsbB variant of *Synechocystis* PCC 6803 cells that was previously developed by Brudvig, Lakshmi, and co-workers was propagated on BG-11-glucose agar plates.[39,40] The cells were grown in 18 L cultures under constant illumination at ∼30 °C using BG-11 medium with 5 mM 2-[tris(hydroxymethyl)-methylamino]-1-ethanesulfonic acid/potassium hydroxide (TES-KOH) and 5 mM glucose (pH 8.2). The cells were harvested in buffer containing 50 mM MES-NaOH, 5 mM $CaCl_2$, and 5 mM $MgCl_2$ (pH 6.0) with 25% (w/v) glycerol. Upon being harvested, the cells were broken using a bead beater (BioSpec, Bartlesville, OK) and processed in the dark to

dx.doi.org/10.1021/bi3012093 | *Biochemistry* 2013, 52, 4781−4790

prepare a detergent-solubilized extract of thylakoid proteins. The extract was suspended in buffer containing 50 mM MES-NaOH, 20 mM $CaCl_2$, and 5 mM $MgCl_2$ (pH 6.0) with 25% (w/v) glycerol and 0.03% (w/v) β-DM in the dark and was subjected to purification on a Ni^{2+}-NTA metal-affinity column (QIAgen, Valencia, CA). The Ni^{2+}-NTA column was washed with a solution of 25% (w/v) glycerol, 5 mM $MgCl_2$, 20 mM $CaCl_2$, 50 mM MES-NaOH (pH 6.0), and 0.03% (w/v) β-DM with 5 mM imidazole. The HT-PSII was eluted with a buffer containing 25% (w/v) glycerol, 5 mM $MgCl_2$, 20 mM $CaCl_2$, 50 mM MES-NaOH (pH 6.0), and 0.03% (w/v) β-DM with 250 mM imidazole.[40] The HT-PSII was desalted using an EconoPac 10 D6 desalting column (Bio-Rad). The isolation and purification of HT-PSII were performed in the dark at 4 °C. The purified HT-PSII was characterized using 12% SDS–PAGE analysis, optical assays, and oxygen evolution measurements. Following this, the HT-PSII was stored in buffer containing 50 mM MES-NaOH, 20 mM $CaCl_2$, and 5 mM $MgCl_2$ (pH 6.0) with 25% (w/v) glycerol and 0.03% (w/v) β-DM at −80 °C in the dark.

Manganese Depletion and Cyanide Treatment of Photosystem II. The purified deuterated PSII and HT-PSII from *S. lividus* and the PsbB variant of *Synechocystis* PCC 6803, respectively, were depleted of manganese (Mn) using a buffer containing 50 mM MES-NaOH, 20 mM $CaCl_2$, and 5 mM $MgCl_2$ (pH 6.0) with 25% (w/v) glycerol, 0.03% (w/v) β-DM, 10 mM hydroxylamine hydrochloride (NH_2OH·HCl), and 10 mM sodium ethylenediaminetetraacetic acid (EDTA).[37,41] The addition of NH_2OH·HCl results in the disassembly of the Mn_4Ca–oxo cluster of PSII. The Mn-depleted PSII complexes were repeatedly washed in a buffer containing 50 mM MES-NaOH, 20 mM $CaCl_2$, and 5 mM $MgCl_2$ (pH 6.0) with 25% (w/v) glycerol, 0.03% (w/v) β-DM, and 5 mM EDTA.

The high-spin (electron spin $S = 2$) non-heme iron center, Fe(II), in Mn-depleted deuterated PSII and Mn-depleted HT-PSII was converted to its low-spin (electron spin $S = 0$) state by incubation with 350 mM potassium cyanide (KCN) at pH 6.0 for 3.5 h in the dark at 4 °C.[42] Although manganese depletion and cyanide (CN) treatment are not required for the observation of the PCET intermediates of $Y_D^\bullet$, these protocols were applied as the deuterated PSII preparation was also used for HF ENDOR spectroscopy experiments with the primary semiquinone, Q_A^-.

The Mn-depleted, CN-treated deuterated PSII was suspended in tricine buffer or "protonated" buffer at pH 8.7. The Mn-depleted, CN-treated HT-PSII was suspended in tricine buffer in D_2O or "deuterated" buffer at pH 8.7.

Photochemical Trapping of the Proton-Coupled Electron Transfer Intermediates of the Y_D Residue of Photosystem II. The early unrelaxed PCET intermediate of Y_D was trapped by illuminating the Mn-depleted, CN-treated deuterated PSII and Mn-depleted, CN-treated HT-PSII from *S. lividus* and the PsbB variant of *Synechocystis* PCC 6803, respectively, at pH 8.7 and 7 K for 2 min using 550 nm laser pulses (~1 mJ/pulse) with a flash frequency of 10 Hz. The late relaxed PCET intermediate of Y_D was trapped by illuminating Mn-depleted, CN-treated deuterated PSII and Mn-depleted, CN-treated HT-PSII at pH 8.7 for 2 min at 240 K, which allows for temperature-induced relaxation. The experimental HF EPR and HF ^{2}H ENDOR spectra of the unrelaxed and relaxed PCET intermediate of Y_D were recorded at 20 K.

Pulsed High-Frequency EPR and ENDOR Spectroscopy. The high-frequency (HF) EPR spectra were obtained on a home-built D-band (130 GHz, 4.5 T) continuous wave (cw)/pulsed spectrometer.[37,43,44] The pulsed HF ENDOR spectra were recorded using a Mims sequence[31] of microwave (MW) and radiofrequency (RF) pulses ($\pi/2_{MW}-\tau-\pi/2_{MW}-\pi_{RF}-\pi/2_{MW}$) by monitoring the electron-spin–echo intensity as a function of the frequency of the RF pulse. The RF pulses were generated by an Agilent RF signal generator (model E4400B) and amplified by a 1 kW pulsed amplifier (CPC, model 5T1000). For the HF ^{2}H ENDOR experiment, the duration of the MW pulses was 60 ns and that of the RF π-pulse was 170 μs. The light excitation of the sample was achieved with an optical parametric oscillator (Opotek, Carlsbad, CA) pumped by a Nd:YAG laser (Quantel, Bozeman, MT), the output of which was coupled to an optical fiber. The optical fiber allows delivery of up to 1 mJ/pulse to the sample. The PSII samples were held in quartz tubes (inside diameter of 0.5 mm and outside diameter of 0.6 mm) and placed in the MW resonator. The resonator was held in an Oxford flow cryostat (Oxford Instruments, Oxford, U.K.). The samples were frozen in the dark in the resonator/cryostat, and the temperature was controlled with an ITC Oxford temperature control system (Oxford Instruments).

Spin–Echo-Detected Magnetic Field-Sweep EPR Spectra of the Relaxed and Unrelaxed PCET Intermediates of $Y_D^\bullet$. The spin–echo-detected magnetic field-sweep EPR spectra of the relaxed and unrelaxed intermediates of the Y_D residue are represented by solid black lines in Figure 1. We used the "pepper" function of the EasySpin software package for numerical simulations of the experimental spectra.[45] In the numerical simulations, we neglected the hyperfine interactions and used an orientation-dependent line broadening parameter "HStrain". For the relaxed intermediate, we reproduce the experimental spectra assuming contributions from three species: the tyrosyl radical, $Y_D^\bullet$, primary semiquinone anion radical, Q_A^-, and a species with much smaller g anisotropy corresponding to the monomeric chlorophyll (Chl_Z^+) and/or β-carotene (Car^+) radical of PSII.[37,46] For the unrelaxed intermediate, a small additional contribution from the relaxed state was added to the simulated spectrum. The principal components of the **g** tensor of all of the species are presented in Table 1.

Table 1. Relative g Tensor of the Unrelaxed and Relaxed PCET Intermediates of $Y_D^\bullet$, Q_A^-, and Chl_Z^+/Car^+ Residues in Mn-Depleted, CN-Treated Deuterated PSII That Were Obtained from the Spectral Simulation of the HF EPR Spectra[a]

cofactor	g_x	g_y	g_z
$Y_D^\bullet$ (unrelaxed)	2.00673	2.00453	2.00232
$Y_D^\bullet$ (relaxed)	2.00774	2.00447	2.00232
Q_A^-	2.0067	2.0052	2.00232
Chl_Z^+/Car^+	2.0031	2.0027	2.00232

[a]The g_z component of the **g** tensor is normalized to the g value of a free electron.

Numerical Simulation of the HF ^{2}H ENDOR Spectra. The numerical simulations of the HF ^{2}H ENDOR spectra were performed with the "salt" function of the EasySpin software package.[45] Orientation selection was achieved by using the **g** tensor determined from the numerical simulations of the spin–echo-detected magnetic field-sweep EPR spectra described above and assuming microwave excitation corresponding to a

dx.doi.org/10.1021/bi3012093 | *Biochemistry* 2013, 52, 4781–4790

rectangular-shaped microwave pulse length of 60 ns. To simulate the experimental spectra of the intrinsic deuterons on the tyrosine residue, we used the data available in the literature as an initial estimate.[47,48] The orientation of the electron−nuclear hyperfine tensors has been described in previously published reports.[47,48] The orientation of the nuclear quadrupole tensor is assumed to be collinear with the electron−nuclear hyperfine tensor.

Determination of the Hydrogen Bond Distance. For the numerical simulations of the hydrogen (H)-bonded deuteron in the relaxed and unrelaxed states, we assumed the H-bond to be in the plane containing the tyrosyl ring of $Y_D^{\bullet}$. This is in agreement with the recently determined high-resolution crystal structure of PSII,[18] in which the τ-nitrogen of D2-His189 is in plane with the tyrosyl ring of Y_D. To reduce the number of variables, we calculated the hyperfine tensor using the McConnell equations that suggest that the unpaired electron is located in the 2p Slater orbital of the oxygen atom:[49]

$$A_x = -\frac{2\rho}{R^3}\left[1 - \frac{9}{a^2} + \left(a^3 + 4a^2 + 10a + 17 + \frac{18}{a} + \frac{9}{a^2}\right)e^{-2a}\right] \quad (1)$$

$$A_y = \frac{1\rho}{R^3}\left[1 - \frac{9}{2a^2} + \left(a^2 + 4a + 8 + \frac{9}{a} + \frac{9}{2a^2}\right)e^{-2a}\right] \quad (2)$$

$$A_z = \frac{1\rho}{R^3}\left[1 - \frac{27}{2a^2} + \left(2a^3 + 7a^2 + 16a + 26 + \frac{27}{a} + \frac{27}{2a^2}\right)e^{-2a}\right] \quad (3)$$

where ρ is the spin density on the oxygen atom and $a = (ZR)/(2a_0)$, where Z is the effective charge of oxygen for the 2p orbital and a_0 is the Bohr radius. The electron spin density on the oxygen atom varies from ~0.24 to 0.34 in tyrosyl radicals, and such changes are most likely due to the presence of a H-bond that can lower the electron spin density.[33,50,51] In this study, a value of 0.28 was selected for the electron spin density on the oxygen atom of $Y_D^{\bullet}$ in both the unrelaxed and relaxed intermediates. The effective charge, Z, was assumed to be 4.45.[52,53] The electron−nuclear interspin distance, R, the angle of the H-bond in the plane of the tyrosyl ring, and the quadrupole tensor were treated as variables in the numerical simulations of the experimental HF ^{2}H ENDOR spectra.

RESULTS AND DISCUSSION

***In Situ* Observation of the PCET Intermediates of $Y_D^{\bullet}$.** This study is focused on understanding the mechanism of the photoinduced PCET reaction that leads to the formation of the redox-active tyrosyl radical, $Y_D^{\bullet}$, of PSII. It has been demonstrated that it is possible to photo-oxidize Y_D at 7 K where both the proton and protein motions are limited.[26,27] This leads to the formation of the low-temperature early unrelaxed PCET intermediate of $Y_D^{\bullet}$. However, illumination of PSII at a higher temperature (240 K) allows for unrestricted proton movement and possibly the relaxation of the protein environment.[26,27] This results in the formation of the late relaxed PCET intermediate of $Y_D^{\bullet}$. Here, we trap the unrelaxed and relaxed PCET intermediates of $Y_D^{\bullet}$ of wild-type Mn-depleted, CN-treated deuterated PSII and Mn-depleted, CN-treated HT-PSII from *S. lividus* and the PsbB variant of *Synechocystis* PCC 6803, respectively. We utilize the enhanced resolution and sensitivity of HF EPR and HF ^{2}H ENDOR spectroscopy[37] to elucidate the structure of the unrelaxed and relaxed PCET intermediates and, hence, the sequence of events during the light-induced PCET reaction at the Y_D residue of PSII.

At high frequencies, the line shape of an EPR spectrum is typically determined by the anisotropy of the Zeeman interaction of the paramagnetic center in the presence of an external magnetic field. This results in an EPR spectrum with three characteristic features corresponding to the direction of the canonical axes of the **g** tensor with respect to the external magnetic field. As one can see in panels A and B of Figure 1,

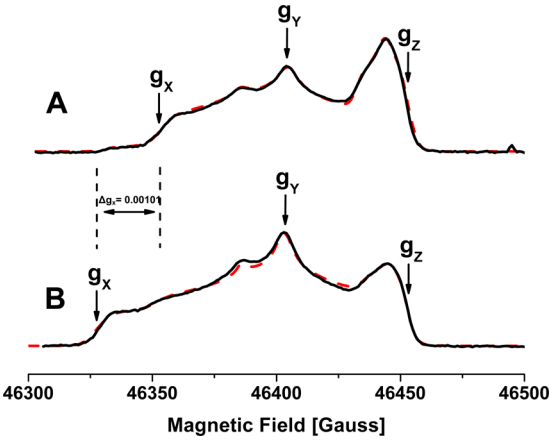

Figure 1. HF 130 GHz spin−echo-detected magnetic field-sweep EPR spectra of Mn-depleted, CN-treated deuterated PSII in protonated buffer in the (A) unrelaxed and (B) relaxed PCET intermediate states. The experimental spectra are shown as solid black traces, and the simulated spectra are shown as dashed red traces. The g_x, g_y, and g_z components of $Y_D^{\bullet}$ are marked by arrows in panels A and B.

the HF EPR spectra of the unrelaxed and relaxed PCET intermediates of Y_D exhibit multiple spectral features. The HF EPR spectra are dominated by features arising from the well-resolved **g** tensor of $Y_D^{\bullet}$ (these are marked by arrows in Figure 1A,B). Also observed are minor additional spectral contributions from other radicals, such as the primary semiquinone (Q_A^-), β-carotene (Car^+), and monomeric chlorophyll (Chl_Z^+) radical of PSII that are easily identified by their characteristic principal g values (Table 1).[37,46,54,55]

Further examination of the EPR spectra of the unrelaxed and relaxed intermediates in panels A and B of Figure 1 and the corresponding **g** tensors presented in Table 1 reveals that the value of the g_x component of $Y_D^{\bullet}$ in the unrelaxed intermediate is 2.00673. However, in the case of the relaxed intermediate of $Y_D^{\bullet}$, the spectral feature corresponding to the g_x component shifts to a lower magnetic field with a value of 2.00774. Thus, there is a significant shift of the g_x component of the $Y_D^{\bullet}$ radical in the unrelaxed and relaxed PCET intermediates. In contrast, numerical simulations indicate that the values of the g_y and g_z components of $Y_D^{\bullet}$ remain identical, within the accuracy of the experiment, in both the unrelaxed and relaxed PCET intermediates. These results confirm an earlier study performed by Faller et al. in which two $Y_D^{\bullet}$ intermediates were reported for the first time.[26,27]

dx.doi.org/10.1021/bi3012093 | *Biochemistry* 2013, 52, 4781−4790

In the case of organic radicals, the anisotropy of the **g** tensor is mostly determined by the spin−orbit coupling interaction at the heavy atom, namely, the oxygen atom in the case of a tyrosyl radical. The spin−orbit coupling interaction arises because of relativistic effects that are significant in heavier atoms. The observed shift of the g_x value in the spin−echo-detected magnetic field-sweep EPR spectra of the unrelaxed and relaxed intermediate shown in panels A and B of Figure 1 reflects significant reduction of the electron spin density at the oxygen atom of the $Y_D^\bullet$ radical. Such a change in the electron spin density can be induced by either a change in the H-bond strength at the carbonyl oxygen atom or conformational changes of the $Y_D^\bullet$ radical. It is thought that the tyrosine-D residue (D2-Tyr160), Y_D, has a single H-bond with the neighboring D2-His189 residue of PSII.[56] An increase in the anisotropy of the **g** tensor upon relaxation of the intermediate at a higher temperature could reflect weakening of the H-bond with the τ-nitrogen of the D2-His189 residue. Recently, Svistunenko et al.[47] analyzed hyperfine parameters that were obtained in previous HF ENDOR spectroscopy studies of tyrosyl radicals of different proteins. This study estimated the rotation angle of the tyrosyl ring of the $Y_D^\bullet$ radical to be ∼50° in PSII.[47] In principle, a significant change in the rotation angle of the tyrosyl ring could also affect the electron spin density distribution of the $Y_D^\bullet$ radical. This could result in the changes that are observed in the *g* anisotropy of the unrelaxed and relaxed PCET intermediate of the Y_D residue of PSII. To directly probe the strength of the H-bond and the rotational conformation of the tyrosyl ring of $Y_D^\bullet$, we performed HF ^{2}H ENDOR spectroscopy on the unrelaxed and relaxed PCET intermediates of $Y_D^\bullet$.

Proton Movement in the PCET Intermediates of $Y_D^\bullet$. To characterize the hydrogen bonding interaction of the unrelaxed and relaxed PCET intermediates of $Y_D^\bullet$, we performed HF ^{2}H ENDOR spectroscopy of protonated Mn-depleted, CN-treated HT-PSII from the PsbB variant of *Synechocystis* PCC 6803 that is exchanged in deuterated buffer (where the buffer is prepared in D_2O). The exchange of protonated Mn-depleted, CN-treated HT-PSII in deuterated buffer results in the replacement of the H-bonded proton with a deuteron[57−61] that facilitates exclusive detection of the electron−nuclear hyperfine interaction of the H-bonded deuteron by HF ^{2}H ENDOR spectroscopy. To obtain quantitative information about the principal components and canonical orientation of the hyperfine tensor in the molecular frame, we conduct HF ^{2}H ENDOR measurements at multiple spectral positions that correspond to different orientations of the **g** tensor with respect to the external magnetic field. In the case of a tyrosyl radical, the HF ^{2}H ENDOR measurements are orientation selective as the microwave excitation bandwidth is much smaller than the *g* anisotropy (and spectral width) of the HF EPR spectrum.

The experimental HF ^{2}H ENDOR spectra of the unrelaxed and relaxed PCET intermediate of $Y_D^\bullet$ are shown in panels A−C of Figure 2. As can be seen in panels A and B, the HF ^{2}H ENDOR spectra that are measured at a magnetic field position corresponding to the g_x component of the **g** tensor display a single well-resolved splitting arising from the electron−nuclear hyperfine interaction of the electron spin with the H-bonded deuteron. In this case, the nuclear quadrupole interaction is much weaker and contributes to the shape of the individual peaks of the doublet in panels A and B of Figure 2. A qualitative comparison of the HF ^{2}H ENDOR spectra at the magnetic field

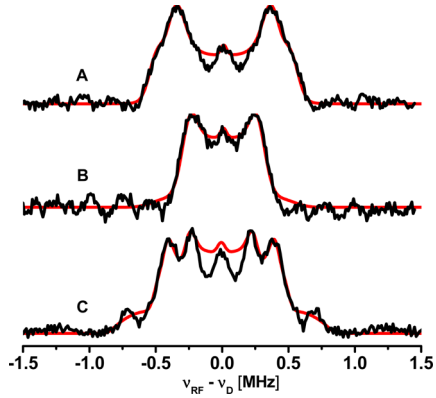

Figure 2. Mims HF ^{2}H ENDOR spectrum of Mn-depleted, CN-treated HT-PSII in deuterated buffer in the (A) g_x orientation of the unrelaxed intermediate and (B) g_x orientation of the relaxed intermediate. (C) Mims HF ^{2}H ENDOR spectrum of Mn-depleted, CN-treated HT-PSII in deuterated buffer in the g_y orientation of the relaxed PCET intermediate. The experimental spectra are depicted as black traces and the simulations as red traces.

position corresponding to the g_x component of the **g** tensor indicates that the hyperfine splitting that is observed in the unrelaxed intermediate (Figure 2A) is larger than the splitting that is observed in the relaxed intermediate (Figure 2B). In contrast with the single well-defined hyperfine splitting that is observed in the HF ^{2}H ENDOR spectra at the magnetic field position corresponding to the g_x component of the **g** tensor (Figure 2A,B), the spectrum that is measured at a magnetic field position corresponding to the g_y component of the **g** tensor of the relaxed intermediate (Figure 2C) is more complex. The spectral complexity arises from the contribution of multiple molecular orientations to the g_y component with respect to the magnetic field.

We performed numerical simulations of the experimental HF ^{2}H ENDOR spectra to obtain quantitative information about the hyperfine components of the H-bonded deuteron in the unrelaxed and relaxed PCET intermediates. To reduce the number of variables in the numerical simulations, we calculated the electron−nuclear hyperfine tensor using McConnell equations (see Materials and Methods).[49] The distance between the carbonyl oxygen and H-bonded proton, the angle of the H-bond in the plane of the tyrosyl ring, the principal components, and the orientation (determined by the Euler angles) of the quadrupole tensor were varied to obtain the best fit with the experimental spectra. The numerical simulations of the experimental HF ^{2}H ENDOR spectra for the unrelaxed and relaxed intermediate are shown as red traces in Figure 2A−C. The principal components of the electron−nuclear hyperfine tensor (A_x, A_y, and A_z), the quadrupole tensor (Q_x, Q_y, and Q_z), and the relative orientation of both tensors in the frame of the **g** tensor are listed in Table 2. To facilitate comparison with previous studies, the values of the principal components of the hyperfine tensor, A_x, A_y, and A_z, have been rescaled for protons, and the proton hyperfine parameters are provided in parentheses. The value of the hyperfine tensor of the H-bonded proton of the relaxed PCET intermediate is in agreement with previous reports on single crystals[58] and frozen solutions of PSII.[57] The hydrogen bonding distance of the relaxed PCET intermediate of $Y_D^\bullet$ is in qualitative agreement with the recent high-resolution X-ray crystal structure of PSII.[18] A quantitative comparison is not possible as the high-resolution

dx.doi.org/10.1021/bi3012093 | *Biochemistry* 2013, 52, 4781−4790

Table 2. Magnetic Parameters Obtained from Numerical Simulations of the Mims HF ^{2}H ENDOR Spectra of Mn-Depleted, CN-Treated HT-PSII in Deuterated Buffer at the g_x Orientation[a]

	A_x (MHz)	A_y (MHz)	A_z (MHz)	$[\alpha, \beta, \gamma]^b$ (deg)	Q_x (MHz)	Q_y (MHz)	Q_z (MHz)	$[\alpha, \beta, \gamma]^b$ (deg)
exchanged deuterons (unrelaxed)	1.59 (10.34)	−0.91 (−5.93)	−0.68 (−4.41)	[108, 0, 0]	0.14	−0.066	−0.074	[126, 0, 0]
exchanged deuterons (relaxed)	1.06 (6.88)	−0.58 (−3.79)	−0.48 (−3.10)	[120, 0, 0]	0.11	−0.04	−0.07	[142, 0, 0]

[a]The hyperfine parameters rescaled for the proton gyromagnetic ratio are provided in parentheses. [b]The Euler rotation angles are defined with respect to the principal axis frame of the **g** tensor.

X-ray crystal structure of PSII does not include coordinates for protons.

We observe a significant decrease in the H-bond distance in the unrelaxed PCET intermediate (1.49 Å) in comparison with that of the relaxed PCET intermediate (1.75 Å) of $Y_D^\bullet$. The change in the interspin distance of the H-bonded deuteron in the unrelaxed and relaxed PCET intermediates of $Y_D^\bullet$ that is observed in this study can be reviewed in the context of the two PCET models that were previously proposed by Faller et al.[26,27] By measuring the pH dependence of tyrosine oxidation rates, we proposed that ET at the Y_D residue is coupled to deprotonation with a pK_a value of ∼7.7. The pH dependences of the rates of ET were explained by two possible PCET pathways for the photoinduced oxidation of the Y_D residue that is thought to occur in concert with a conjugate base, D2-His189. In the first pathway, abstraction of a proton from the carbonyl oxygen by the D2-His189 residue is proposed occur prior to ET from the Y_D residue. In this case, a strong interaction between the carbonyl oxygen atom and the H-bonded proton (at a distance estimate of 1.58 Å) has been predicted in the initial unrelaxed His-Tyr$^\bullet$ intermediate. Subsequent temperature-induced thermal relaxation by the motion of the histidine residue is predicted to increase the distance between the carbonyl oxygen atom and the H-bonded proton to 1.93 Å in the relaxed intermediate. In the second pathway, abstraction of a proton by the D2-His189 residue is proposed to either follow or occur simultaneously with ET from the Y_D residue. The distance between the carbonyl oxygen atom and the H-bonded proton has been predicted to be 1.85 Å in the unrelaxed His-Tyr$^\bullet$ intermediate. In this case, upon temperature-induced thermal relaxation of the histidine residue, the H-bond length is proposed to increase only slightly from 1.85 to ∼1.93 Å. The significant difference in the H-bond distances in these two possible pathways originates from the fact that the τ-nitrogen atom of the deprotonated D2-His189 residue is expected to be <2.60 Å from the carbonyl oxygen of the Y_D residue in comparison with the distance in the protonated D2-His189 residue (2.82 Å).

The results of this study do not support the second pathway, in which proton abstraction by D2-His189 is proposed to accompany ET from the Y_D residue. The change in distance of 0.26 Å that is observed in the HF ENDOR experiments is too large in comparison with the predicted change of 0.08 Å in the theoretical model. The larger change in distance of 0.35 Å that is predicted for the first pathway is in reasonable agreement with the experimental observations in this study. The smaller value obtained experimentally could be due to increased electron spin density on the oxygen atom of the carbonyl group in the relaxed state. However, in the numerical calculations, we assumed a fixed value of the electron spin density in both the unrelaxed and relaxed intermediate. An increase in the value of the electron spin density would result in an underestimation of the H-bond length in the relaxed intermediate in comparison with that in the unrelaxed intermediate.

A recent study by Hienerwadel et al. has suggested that Y_D remains protonated in the pH range of 6.0−10.0 and the protonation state of the D2-His189 residue remains unchanged at these pH values.[62] Thus, the first pathway that suggested deprotonation of Y_D prior to electron transfer is in disagreement with the results of the FTIR study. However, the second pathway that suggested that the oxidation of Y_D is promoted at higher pH values by the deprotonation of the D2-His189 residue is also in disagreement with the FTIR study.

The short distance that is observed between the proton and carbonyl oxygen of $Y_D^\bullet$ in the unrelaxed state (1.49 Å) in this study indicates the proximity of the hydrogen bonding partner at pH 8.7. This observation is in agreement with the FTIR study that suggested the involvement of Y_D in very strong hydrogen bonding interaction at pH >7.5.[62] The contradictions between the theoretical models and FTIR spectroscopy data could arise from the fact that additional amino acid residues impact the structure and function of the Y_D−D2-His189 couple *in vivo*. Thus, it remains unclear whether the formation of the unrelaxed intermediate is preceded by a tyrosinate moiety at pH >7.5, D2-His189 remains as the H-bonding partner of Y_D, or another residue is involved in the formation of the very strong bond. These questions will be further addressed in future investigations.

For the relaxed PCET intermediate of $Y_D^\bullet$, the numerical simulations yield an angle of 120 ± 10° between the H-bond and C−O bond of the carbonyl group. This is reasonable because the sp^2-hybridized oxygen has a lone pair orbital that is in the ring plane and makes an angle of 120° with respect to the C−O axis. For carbonyl radicals, there is a noticeable preference for the H-bond to be in the direction of the lone pair at an angle of ∼120°.[63] Thus, in the case of a carbonyl group, the orientation of the H-bonded proton is expected to be close to this angle. In a recent theoretical study, Brynda et al.[64] calculated the angle of the optimized Tyr-His structure to be 124°, which is in excellent agreement with our finding. Similarly, from numerical simulations, the H-bond angle for the unrelaxed $Y_D^\bullet$ intermediate is estimated to be 108 ± 20°. This suggests that there is negligible change in the angle between the H-bond and C−O bond of the carbonyl group in the relaxed and unrelaxed intermediates. The orientation of the H-bond of the relaxed $Y_D^\bullet$ intermediate that is determined in this study is in excellent agreement with the recent high-resolution X-ray crystal structure of PSII.[18]

Conformation of the Tyrosyl Ring in the PCET Intermediates of $Y_D^\bullet$. To probe the conformation of the tyrosyl ring in the unrelaxed and relaxed intermediate of the Y_D residue, we perform HF ^{2}H ENDOR spectroscopy on Mn-depleted CN-treated deuterated PSII from *S. lividus* in protonated buffer (where the buffer is prepared in H_2O). In this case, the hyperfine interactions with the intrinsic deuterons

dx.doi.org/10.1021/bi3012093 | *Biochemistry* 2013, 52, 4781−4790

of the tyrosyl radical, $Y_D^{\bullet}$, contribute to the experimental HF ^{2}H ENDOR spectra. As shown in Figure 3A–D, the HF ^{2}H

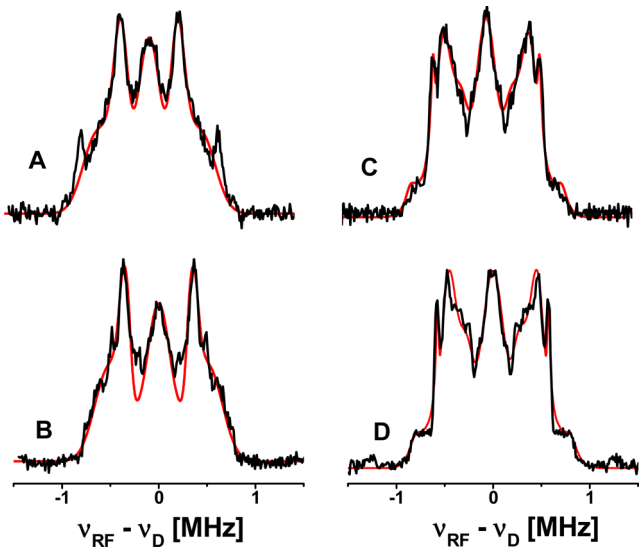

Figure 3. Mims HF ^{2}H ENDOR spectrum of Mn-depleted, CN-treated deuterated PSII in protonated buffer in the (A) g_x orientation of the unrelaxed intermediate, (B) g_x orientation of the relaxed intermediate, (C) g_y orientation of the unrelaxed intermediate, and (D) g_y orientation of the relaxed intermediate. The experimental spectra are depicted as black traces and the simulations as red traces.

ENDOR spectra for the unrelaxed and relaxed intermediate are measured at magnetic field positions that correspond to the g_x and g_y components of the **g** tensor, respectively. We observe that the spectral line shapes are determined by the hyperfine interaction of the unpaired electron with the four deuterons on the ring and the β-methylene deuterons of the tyrosyl radical (Figure 4A,B). To obtain quantitative information about the hyperfine interactions with the deuterons, we perform numerical simulations of the HF ^{2}H ENDOR spectra. The hyperfine parameters of the numerical simulations were adjusted to obtain the best fit with the experimental spectra.

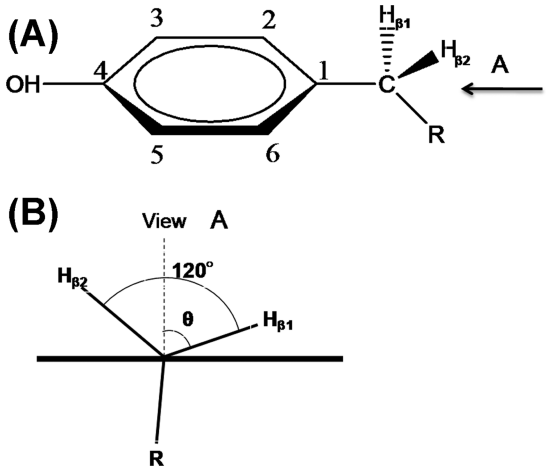

Figure 4. (A) Schematic depicting the definition of the rotation angle, θ, of the tyrosine ring plane as defined in this study. (B) View where the angle, θ, for proton β_1 increases when it is measured clockwise from the perpendicular to the ring plane when the C_β–R bond is below the horizontally oriented ring plane.

An initial estimate of the simulation parameters and assignment of the observed spectral features were obtained from the literature on the hyperfine tensors of the intrinsic protons of the relaxed intermediate.[47,48] In this analysis, we assume that the pairs of deuterons at positions 2 and 6 and positions 3 and 5 of the tyrosyl ring have identical hyperfine components within the pair. Although a recent single-crystal EPR spectroscopy study suggests that this is not the case,[65] the differences between the hyperfine components are too small to be resolved in powder samples of a frozen solution.

The spectral features that are observed in the HF ^{2}H ENDOR spectra shown in Figure 3A–D arise from hyperfine interactions with the deuterons at positions 2 and 6 of the tyrosyl ring and one deuteron at the β-methylene position, β_1. The ring deuterons at positions 3 and 5 of the tyrosyl ring have negligible contributions to the HF ^{2}H ENDOR spectra. This is due to the large anisotropy of the hyperfine tensor that precludes detection under the experimental conditions of the HF ^{2}H ENDOR experiment. Similarly, a contribution from the second β-methylene proton, β_2, is not observed in the HF ^{2}H ENDOR spectra because the hyperfine interaction of β_2 with the unpaired electron is too strong to be detected under these experimental conditions. The hyperfine parameters, the electron–nuclear hyperfine tensor (A_x, A_y, A_z), and the nuclear quadrupole tensor (Q_x, Q_y, Q_z) that are obtained from the numerical simulations are listed in Table 3. The values of principal hyperfine components, A_x, A_y, and A_z, have been rescaled for the proton gyromagnetic ratio, and the proton hyperfine parameters are provided in parentheses.

It is important to note here that contributions from the intrinsic protons of the primary semiquinone (Q_A^-), β-carotene (Car^+), or monomeric chlorophyll (Chl_Z^+) radical are not detected in the HF ^{2}H ENDOR spectra shown in Figure 3A–D. This confirms our earlier assumption that the observed HF ^{2}H ENDOR features in Figure 2A–C are entirely due to the $Y_D^{\bullet}$ radical and possible contributions from other unwanted radicals is negligible.

To relate the obtained parameters to a certain conformation of the radical, we utilize the McConnell equation that expresses the isotropic component of the hyperfine tensor of a β-methylene proton via the unpaired electron spin density at C_1 (Figure 4A) and the dihedral angle, θ, the angle between the plane perpendicular to the tyrosyl ring and the plane containing C_1, C_β, and $H_{\beta1}$, as shown in Figure 4B.[66]

$$A_{iso}^{\beta_1} = \rho_{C_1}(B' + B'' \cos^2 \theta) \quad (4)$$

where $A_{iso}^{\beta_1}$ is the isotropic hyperfine constant of the corresponding β-methylene proton, ρ_{C_1} is the spin density on atom C_1, and B' and B'' are constants. B' is neglected in practical applications, and B'' is known to be 58 G.[67] The angle of the second β-methylene proton can be easily evaluated taking into account that its dihedral angle is shifted by 120° (Figure 4B). The electron spin density, ρ_{C_1}, on atom C_1 has been estimated to be 0.37.[68] Although eq 4 was derived for protons, it can be used for deuterons by simply using a scaling factor of 6.51 for the corresponding hyperfine components. Using the isotropic hyperfine component value of 9.2 MHz that is obtained from the numerical simulations, eq 2 yields a dihedral angle of 67.0° for the β_1-methylene deuteron in the relaxed intermediate. This value is in excellent agreement with previous studies of the relaxed state.[47,69] The dihedral angle of the β-methylene deuteron for the relaxed intermediate of Y_D

dx.doi.org/10.1021/bi3012093 | *Biochemistry* 2013, 52, 4781–4790

Table 3. Magnetic Parameters Obtained from Numerical Simulations of the Mims HF ^{2}H ENDOR Spectra of Mn-Depleted, CN-Treated Deuterated PSII in Protonated Buffer in the g_x Orientation[a]

	A_x (MHz)	A_y (MHz)	A_z (MHz)	$[\alpha, \beta, \gamma]^b$ (deg)	Q_x (MHz)	Q_y (MHz)	$[\alpha, \beta, \gamma]^b$ (deg)
β_1 proton (unrelaxed)	0.92 (6.0)	1.09 (7.1)	2.22 (14.5)	[0, 0, 0]	0.07	0.14	[0, 0, 0]
β_1 proton (relaxed)	0.84 (5.5)	1.14 (7.45)	2.38 (15.5)	[0, 0, 0]	0.07	0.08	[0, 0, 0]
C2/C6 (unrelaxed)	0.55 (3.6)	1.01 (6.6)	0.34 (2.2)	[±10, 0, 0]	0.02	0.015	[±10, 0, 0]
C2/C6 (relaxed)	0.69 (4.5)	1.03 (6.7)	0.28 (1.8)	[±10, 0, 0]	0.02	0.015	[±10, 0, 0]

[a]The hyperfine parameters rescaled for the proton gyromagnetic ratio are provided in parentheses. [b]The Euler rotation angles are defined with respect to the principal axis frame of the **g** tensor.

that is determined in this study is also in excellent agreement with the recent high-resolution X-ray crystal structure of PSII.[18] The value of the dihedral angle for the unrelaxed intermediate is calculated to be 66.6°. Because the dihedral angles for the unrelaxed and relaxed PCET intermediate are virtually identical, we can conclude that the conformation of the tyrosyl ring is similar in both of the intermediates. This suggests that there is no change in the conformation of the tyrosyl ring upon temperature-induced relaxation from the unrelaxed PCET intermediate to the relaxed state. This conclusion confirms the argument made in a recent study by Faller et al., who suggest no conformational changes based on observation of the largest hyperfine component of a β-methylene proton.[27]

CONCLUSIONS

In this study, we trap two light-induced intermediate states of the Y_D residue of PSII, namely, the unrelaxed and relaxed PCET intermediate.[27] We observe an increase in the g anisotropy upon temperature-induced relaxation of the unrelaxed intermediate to the relaxed state as reported by Faller et al.[26,27] This observation indicates the presence of possible structural differences between the two intermediates. We probe the differences by performing HF ^{2}H ENDOR spectroscopy experiments. On the basis of numerical simulations of the experimental HF ^{2}H ENDOR spectra, we observe a significant change in the H-bond length of the tyrosyl radical in the unrelaxed and relaxed PCET intermediates. The distance between carbonyl oxygen and the H-bonded proton is estimated to be 1.49 Å in the unrelaxed intermediate. Such a short distance indicates the presence of a very strong H-bonding interaction of the Y_D residue during its oxidation. The measurement of the hyperfine parameters of the β-methylene protons indicates that there are negligible changes in the conformation of the tyrosyl ring in the unrelaxed and relaxed PCET intermediates of $Y_D^{\bullet}$. The presence of a strong H-bonding interaction of the Y_D residue during its oxidation and the thermal relaxation of the conjugate base provide direct experimental insight into individual events that accompany light-induced PCET at the Y_D residue at cryogenic temperatures. Importantly, the parameters determined in this study facilitate the prediction of theoretical models for the PCET reactions at the Y_D residue.

AUTHOR INFORMATION

Corresponding Author

*E-mail: lakshk@rpi.edu. Phone: (518) 276-3271. Fax: (518) 276-4887.

Funding

This work was supported by the U.S. Department of Energy, Office of Basic Energy Sciences, Division of Chemical Sciences, Geosciences, and Biosciences, and the Photosynthetic Systems Program under Contracts DE-FG02-07ER15903 (K.V.L.) and DE-AC02-06CH11357 (O.G.P.).

Notes

The authors declare no competing financial interest.

REFERENCES

(1) Nicholls, D. G., and Ferguson, S. J. (2002) *Bioenergetics 3*, Academic Press, New York.

(2) Wraight, C. A. (2005) *Intraprotein proton transfer: Concepts and realities from the bacterial photosynthetic reaction center*, Royal Society of Chemistry, London.

(3) Cukier, R. I., and Nocera, D. G. (1998) Proton-coupled electron transfer. *Annu. Rev. Phys. Chem. 49*, 337−369.

(4) McEvoy, J. P., and Brudvig, G. W. (2006) Water-splitting chemistry of photosystem II. *Chem. Rev. 106*, 4455−4483.

(5) Rutherford, A. W. (1989) Photosystem-II, the water-splitting enzyme. *Trends Biochem. Sci. 14*, 227−232.

(6) Yachandra, V. K., Sauer, K., and Klein, M. P. (1996) Manganese cluster in photosynthesis: Where plants oxidize water to dioxygen. *Chem. Rev. 96*, 2927−2950.

(7) Tommos, C., and Babcock, G. T. (1998) Oxygen production in nature: A light-driven metalloradical enzyme process. *Acc. Chem. Res. 31*, 18−25.

(8) Babcock, G. T., Barry, B. A., Debus, R. J., Hoganson, C. W., Atamian, M., McIntosh, L., Sithole, I., and Yocum, C. F. (1989) Water oxidation in photosystem 2 from radical chemistry to multielectron chemistry. *Biochemistry 28*, 9557−9565.

(9) Hansson, O., and Wydrzynski, T. (1990) Current perceptions of Photosystem-II. *Photosynth. Res. 23*, 131−162.

(10) Tommos, C., and Babcock, G. T. (2000) Proton and hydrogen currents in photosynthetic water oxidation. *Biochim. Biophys. Acta 1458*, 199−219.

(11) Westphal, K. L., Tommos, C., Cukier, R. I., and Babcock, G. T. (2000) Concerted hydrogen-atom abstraction in photosynthetic water oxidation. *Curr. Opin. Plant Biol. 3*, 236−242.

(12) Debus, R. J. (1992) The manganese and calcium ions of photosynthetic oxygen evolution. *Biochim. Biophys. Acta 1102*, 269−352.

(13) Zouni, A., Witt, H. T., Kern, J., Fromme, P., Krauss, N., Saenger, W., and Orth, P. (2001) Crystal structure of photosystem II from *Synechococcus elongatus* at 3.8 angstrom resolution. *Nature 409*, 739−743.

(14) Kern, J., Loll, B., Zouni, A., Saenger, W., Irrgang, K. D., and Biesiadka, J. (2005) Cyanobacterial photosystem II at 3.2 angstrom resolution: The plastoquinone binding pockets. *Photosynth. Res. 84*, 153−159.

(15) Loll, B., Kern, J., Saenger, W., Zouni, A., and Biesiadka, J. (2005) Towards complete cofactor arrangement in the 3.0 angstrom resolution structure of photosystem II. *Nature 438*, 1040−1044.

(16) Ferreira, K. N., Iverson, T. M., Maghlaoui, K., Barber, J., and Iwata, S. (2004) Architecture of the photosynthetic oxygen-evolving center. *Science 303*, 1831−1838.

(17) Kamiya, N., and Shen, J. R. (2003) Crystal structure of oxygen-evolving photosystem II from *Thermosynechococcus vulcanus* at 3.7-angstrom resolution. *Proc. Natl. Acad. Sci. U.S.A. 100*, 98−103.

(18) Umena, Y., Kawakami, K., Shen, J. R., and Kamiya, N. (2011) Crystal structure of oxygen-evolving photosystem II at a resolution of 1.9 angstrom. *Nature 473*, 55−60.
(19) Guskov, A., Kern, J., Gabdulkhakov, A., Broser, M., Zouni, A., and Saenger, W. (2009) Cyanobacterial photosystem II at 2.9-angstrom resolution and the role of quinones, lipids, channels and chloride. *Nat. Struct. Mol. Biol. 16*, 334−342.
(20) Koulougliotis, D., Tang, X. S., Diner, B. A., and Brudvig, G. W. (1995) Spectroscopic evidence for the symmetrical location of tyrosine-D and tyrosine-Z in photosystem II. *Biochemistry 34*, 2850−2856.
(21) Styring, S., and Rutherford, A. W. (1987) In the oxygen-evolving complex of photosystem II the S_0 state is oxidized to S_1 state by D^+ (signal-II slow). *Biochemistry 26*, 2401−2405.
(22) Tracewell, C. A., and Brudvig, G. W. (2003) Two redox-active β-carotene molecules in photosystem II. *Biochemistry 42*, 9127−9136.
(23) Diner, B. A., and Rappaport, F. (2002) Structure, dynamics, and energetics of the primary photochemistry of photosystem II of oxygenic photosynthesis. *Annu. Rev. Plant Biol. 53*, 551−580.
(24) Vrettos, J. S., Limburg, J., and Brudvig, G. W. (2001) Mechanism of photosynthetic water oxidation: Combining biophysical studies of photosystem II with inorganic model chemistry. *Biochim. Biophys. Acta 1503*, 229−245.
(25) Hoganson, C. W., and Babcock, G. T. (1997) A metalloradical mechanism for the generation of oxygen from water in photosynthesis. *Science 277*, 1953−1956.
(26) Faller, P., Rutherford, A. W., and Debus, R. J. (2002) Tyrosine D oxidation at cryogenic temperature in photosystem II. *Biochemistry 41*, 12914−12920.
(27) Faller, P., Goussias, C., Rutherford, A. W., and Un, S. (2003) Resolving intermediates in biological proton-coupled electron transfer: A tyrosyl radical prior to proton movement. *Proc. Natl. Acad. Sci. U.S.A. 100*, 8732−8735.
(28) Lakshmi, K. V., and Brudvig, G. W. (2000) *Electron paramagnetic resonance distance measurements in photosystems*, Kluwer Academic/Plenum Publishers, New York.
(29) Lakshmi, K. V., and Brudvig, G. W. (2001) Pulsed electron paramagnetic resonance methods for macromolecular structure determination. *Curr. Opin. Struct. Biol. 11*, 523−531.
(30) Prisner, T., Rohrer, M., and MacMillan, F. (2001) Pulsed EPR spectroscopy: Biological applications. *Annu. Rev. Phys. Chem. 52*, 279−313.
(31) Mims, W. B. (1965) Pulsed ENDOR experiments. *Proc. R. Soc. London, Ser. A 283*, 452−457.
(32) Un, S., Tang, X. S., and Diner, B. A. (1996) 245 GHz high-field EPR study of tyrosine-D degrees and tyrosine-Z degrees in mutants of photosystem II. *Biochemistry 35*, 679−684.
(33) Farrar, C. T., Gerfen, G. J., Griffin, R. G., Force, D. A., and Britt, R. D. (1997) Electronic structure of the Y-D tyrosyl radical in photosystem II: A high-frequency electron paramagnetic resonance spectroscopic and density functional theoretical study. *J. Phys. Chem. B 101*, 6634−6641.
(34) Un, S., Dorlet, P., and Rutherford, A. W. (2001) A high-field EPR tour of radicals in photosystems I and II. *Appl. Magn. Reson. 21*, 341−361.
(35) Un, S., Atta, M., Fontecave, M., and Rutherford, A. W. (1995) G-values as a probe of the local protein environment: High-field EPR of tyrosyl radicals in ribonucleotide reductase and photosystem-II. *J. Am. Chem. Soc. 117*, 10713−10719.
(36) Wilson, J. C., Wu, G., Tsai, A. L., and Gerfen, G. J. (2005) Determination of the structural environment of the tyrosyl radical in prostaglandin H-2 synthase-1: A high frequency ENDOR/EPR study. *J. Am. Chem. Soc. 127*, 1618−1619.
(37) Lakshmi, K. V., Reifler, M. J., Brudvig, G. W., Poluektov, O. G., Wagner, A. M., and Thurnauer, M. C. (2000) High-field EPR study of carotenoid and chlorophyll cation radicals in photosystem II. *J. Phys. Chem. B 104*, 10445−10448.
(38) Tang, X. S., and Diner, B. A. (1994) Biochemical and spectroscopic characterization of a new oxygen-evolving photosystem II core complex from the cyanobacterium *Synechocystis* PCC6803. *Biochemistry 33*, 4594−4603.
(39) Rippka, R., Deruelles, J., Waterbury, J. B., Herdman, M., and Stanier, R. Y. (1979) Generic assignments, strain histories and properties of pure cultures of cyanobacteria. *J. Gen. Microbiol. 111*, 1−61.
(40) Lakshmi, K. V., Reifler, M. J., Chisholm, D. A., Wang, J. Y., Diner, B. A., and Brudvig, G. W. (2002) Correlation of the cytochrome c_{550} content of cyanobacterial photosystem II with the EPR properties of the oxygen-evolving complex. *Photosynth. Res. 72*, 175−189.
(41) Tamura, N., and Cheniae, G. (1987) Photoactivation of the water-oxidizing complex in photosystem II membranes depleted of Mn and extrinsic proteins. 1. Biochemical and kinetic characterization. *Biochim. Biophys. Acta 890*, 179−194.
(42) Deligiannakis, Y., and Rutherford, A. W. (1998) Reaction centre photochemistry in cyanide-treated photosystem II. *Biochim. Biophys. Acta 1365*, 354−362.
(43) Poluektov, O. G., Paschenko, S. V., Utschig, L. M., Lakshmi, K. V., and Thurnauer, M. C. (2005) Bidirectional electron transfer in photosystem I: Direct evidence from high-frequency time-resolved EPR spectroscopy. *J. Am. Chem. Soc. 127*, 11910−11911.
(44) Poluektov, O. G., Paschenko, S. V., and Utschig, L. M. (2009) Spin-dynamics of the spin-correlated radical pair in photosystem I. Pulsed time-resolved EPR at high magnetic field. *Phys. Chem. Chem. Phys. 11*, 6750−6756.
(45) Stoll, S., and Schweiger, A. (2006) EasySpin, a comprehensive software package for spectral simulation and analysis in EPR. *J. Magn. Reson. 178*, 42−55.
(46) Faller, P., Rutherford, A. W., and Un, S. (2000) High-frequency EPR study of carotenoid and the angular orientation of chlorophyll-z in photosystem II. *J. Phys. Chem. B 104*, 10960−10963.
(47) Svistunenko, D. A., and Cooper, C. E. (2004) A new method of identifying the site of tyrosyl radicals in proteins. *Biophys. J. 87*, 582−595.
(48) Hoganson, C. W., and Babcock, G. T. (1992) Protein tyrosyl radical interactions in photosystem-II studied by electron-spin-resonance and electron nuclear double-resonance spectroscopy: Comparison with ribonucleotide reductase and in vitro tyrosine. *Biochemistry 31*, 11874−11880.
(49) McConnell, H. M., and Strathdee, J. (1959) Theory of anisotropic hyperfine interactions in π-electron radicals. *Mol. Phys. 2*, 129−138.
(50) Dole, F., Diner, B. A., Hoganson, C. W., Babcock, G. T., and Britt, R. D. (1997) Determination of the electron spin density on the phenolic oxygen of the tyrosyl radical of photosystem II. *J. Am. Chem. Soc. 119*, 11540−11541.
(51) van Dam, P. J., Willems, J. P., Schmidt, P. P., Potsch, S., Barra, A. L., Hagen, W. R., Hoffman, B. M., Andersson, K. K., and Graslund, A. (1998) High-frequency EPR and pulsed Q-Band ENDOR studies on the origin of the hydrogen bond in tyrosyl radicals of ribonucleotide reductase R2 proteins from mouse and herpes simplex virus type 1. *J. Am. Chem. Soc. 120*, 5080−5085.
(52) Clementi, E., and Raimondi, D. L. (1963) Atomic screening constants from SCF functions. *J. Chem. Phys. 38*, 2686−2689.
(53) Clementi, E., Raimondi, D. L., and Reinhard., W. P. (1967) Atomic screening constants from SCF functions. 2. Atoms with 37 to 86 electrons. *J. Chem. Phys. 47*, 1300−1306.
(54) Dorlet, P., Rutherford, A. W., and Un, S. (2000) Orientation of the tyrosyl D, pheophytin anion, and semiquinone Q_A^- radicals in photosystem II determined by high-field electron paramagnetic resonance. *Biochemistry 39*, 7826−7834.
(55) Chatterjee, R., Coates, C. S., Milikisiyants, S., Poluektov, O. G., and Lakshmi, K. V. (2012) Structure and function of quinones in biological solar energy transduction: A high-frequency D-band EPR spectroscopy study of model benzoquinones. *J. Phys. Chem. B 116*, 676−682.
(56) Campbell, K. A., Peloquin, J. M., Diner, B. A., Tang, X. S., Chisholm, D. A., and Britt, R. D. (1997) The tau-nitrogen of D2

histidine 189 is the hydrogen bond donor to the tyrosine radical Y-D of photosystem II. *J. Am. Chem. Soc. 119*, 4787−4788.
(57) Force, D. A., Randall, D. W., Britt, R. D., Tang, X. S., and Diner, B. A. (1995) H-2 ESE-ENDOR study of hydrogen bonding to the tyrosine radicals Y-D and Y-Z of photosystem II. *J. Am. Chem. Soc. 117*, 12643−12644.
(58) Kessen, S., Teutloff, C., Kern, J., Zouni, A., and Bittl, R. (2010) High-Field H-2-Mims-ENDOR Spectroscopy on PSII Single Crystals: Hydrogen Bonding of Y-D. *ChemPhysChem 11*, 1275−1282.
(59) Tang, X. S., Chisholm, D. A., Dismukes, G. C., Brudvig, G. W., and Diner, B. A. (1993) Spectroscopic evidence from site-directed mutagenesis of *Synechocystis* PCC6803 in favor of a close interaction between histidine-189 and redox active tyrosine-160 both of polypeptide-D2 of the photosystem II reaction center. *Biochemistry 32*, 13742−13748.
(60) Mino, H., Satoh, J., Kawamori, A., Toriyama, K., and Zimmermann, J. L. (1993) Matrix ENDOR of tyrosine D^+ in oriented photosystem-II membranes. *Biochim. Biophys. Acta 1144*, 426−433.
(61) Evelo, R. G., Hoff, A. J., Dikanov, S. A., and Tyryshkin, A. M. (1989) An ESEEM study of the oxidized electron-donor of plant photosystem-II: Evidence that $D^{\bullet}$ is a neutral tyrosine radical. *Chem. Phys. Lett. 161*, 479−484.
(62) Hienerwadel, R., Diner, B. A., and Berthomieu, C. (2008) Molecular origin of the pH dependence of tyrosine D oxidation kinetics and radical stability in photosystem II. *Biochim. Biophys. Acta 1777*, 525−531.
(63) Braga, D., Grepioni, F., Biradha, K., Pedireddi, V. R., and Desiraju, G. R. (1995) Hydrogen-bonding in organometallic crystals. 2. C-H···O hydrogen-bonds in bridged and terminal first-row metal-carbonyls. *J. Am. Chem. Soc. 117*, 3156−3166.
(64) Brynda, M., and Britt, R. D. (2007) Density functional theory calculations on the magnetic properties of the model tyrosine radical-histidine complex mimicking tyrosyl radical Y-D in photosystem II. *Res. Chem. Intermed. 33*, 863−883.
(65) Teutloff, C., Pudollek, S., Kessen, S., Broser, M., Zouni, A., and Bittl, R. (2009) Electronic structure of the tyrosine D radical and the water-splitting complex from pulsed ENDOR spectroscopy on photosystem II single crystals. *Phys. Chem. Chem. Phys. 11*, 6715−6726.
(66) McConnell, H. M., and Chesnut, D. B. (1958) Theory of isotropic hyperfine interactions in π-electron radicals. *J. Chem. Phys. 28*, 107−117.
(67) Fessenden, R. W., and Schuler, R. H. (1963) Electron spin resonance studies of transient alkyl radicals. *J. Chem. Phys. 39*, 2147−2195.
(68) Warncke, K., Babcock, G. T., and McCracken, J. (1994) Structure of the Y-D tyrosine radical in photosystem-II as revealed by ^{2}H electron-spin echo envelope modulation (ESEEM) spectroscopic analysis of hydrogen hyperfine interactions. *J. Am. Chem. Soc. 116*, 7332−7340.
(69) Nieuwenhuis, S. A. M., Hulsebosch, R. J., Raap, J., Gast, P., Lugtenburg, J., and Hoff, A. J. (1998) Structure of the Y-D tyrosine radical in photosystem II. Determination of the orientation of the phenoxyl ring by enantioselective deuteration of the methylene group. *J. Am. Chem. Soc. 120*, 829−830.